IEEE Access
Multidisciplinary | Rapid Review | Open Access Journal

Date of submission 1 Oct. 2020

Digital Object Identifier ...

Common-Aperture Sub-6 GHz and Millimeter-wave 5G Antenna System

MUHAMMAD IKRAM[1], (Student Member, IEEE), NGHIA NGUYEN-TRONG[1], (Member, IEEE), and AMIN ABBOSH[1],(Senior Member, IEEE)

[1]School of Information Technology and Electrical Engineering, The University of Queensland (UQ), Brisbane, 4072 Australia.

Corresponding author: Muhammad Ikram (e-mail: m.ikram@uq.edu.au).

ABSTRACT The realization of a common-aperture (or shared-aperture) 5G antenna system is proposed for compact and integrated wireless devices. As a combination of a dipole and tapered slots, an integrated antenna design, which operates at multi-bands, i.e. sub-6 GHz at 3.6 GHz and mm-wave at 28 GHz, is validated. The antenna design procedure starts with a dipole operating at 3.6 GHz, which is fed by a modified balun consisting of a tapered slot and a microstrip line. Here, the tapered slot has a dual feature, i.e., it is used to excite the dipole at 3.6 GHz and works as a tapered slot antenna at 28 GHz. Only a single feeder is optimized and used for both structures making the design unique and provides an extremely large frequency ratio. Moreover, the dipole's arms are utilized as an antenna footprint for two tapered slot mm-wave arrays, making the dipole dual-functional. The tapered slot antenna and the mm-wave arrays are optimized in a way that the main beams point at different directions. By this configuration, the design is able to cover an angle of 120^o of space in $\theta-$direction. As a proof of concept, a prototype is fabricated on Rogers RO-5880 with an overall size of $75 \times 25 \times 0.254$ mm^3. The simulated and measured results confirm the validity of the proposed concept.

INDEX TERMS Antenna array, dipole antenna, microwaves, mm-waves, tapered slot, 5G.

I. INTRODUCTION

EXISTING sub-6 GHz wireless communication technologies, i.e. 4G and WiFi, are congested and only allow limited bandwidth and thus, are able to support only limited data rates [1]. To enhance the data rates and improve the system capacity, the next generation of technology, which is known as 5G, must be deployed with a new mechanism of spectrum allocation that allows wider bandwidth [2]. The international telecommunication union (ITU) and Federal communication commission (FCC) have proposed mm-wave band with at least 500 MHz bandwidth for 5G applications [3]. Hence, the integration and compatibility of the existing technology (sub-6 GHz) with the new one (mm-wave) is indispensable.

The mm-wave technology needs high gain antennas to compensate for high path loss. Since the gain is inversely proportional to the width of a radiation beam, high-gain antennas yield narrow beamwidth. Thus, beam scanning is required to improve space coverage. Although the incorporation of phased arrays can achieve beam scanning, they are typically narrow-band, expensive, complicated due to the usage of phase shifters, and require more space to install in modern wireless terminals [4]–[6]. Consequently, multi-port antennas, which allow multiple directive beams pointing specific direction to cover large area of space, provide an alternative solution to phased arrays [7]–[9]. To excite those multi-port antennas, discrete switches based frond-end module can be used instead of phase shifters or other beam switching mechanisms such as Butler matrix [7].

Achieving multi-standard operations with a compact antenna structure is an elusive challenge [10]. According to this requirement, several sophisticated designs have been presented at sub-6 GHz and mm-wave bands [11]–[16]. Although all of them were able to cover sub-6 GHz and mm-wave bands, they provide a single fixed beam at mm-wave bands. Some recent reported shared-aperture designs were able to scan the beam at mm-wave bands by either utilizing phase shifter [17] or leaky wave antenna concept [18]. Nevertheless, leaky wave antennas are typically unable to provide multi-beams at single frequency. Moreover, multiple beams at mm-wave band were also achieved utilizing a dual-functional slot concept via multiple-input multiple-out (MIMO) configurations [19], [20]. However, [19] had bi-directional radiation patterns and [20] was not a shared-

This article has been accepted for publication in a future issue of this journal, but has not been fully edited. Content may change prior to final publication. Citation information: DOI 10.1109/ACCESS.2020.3034887, IEEE Access

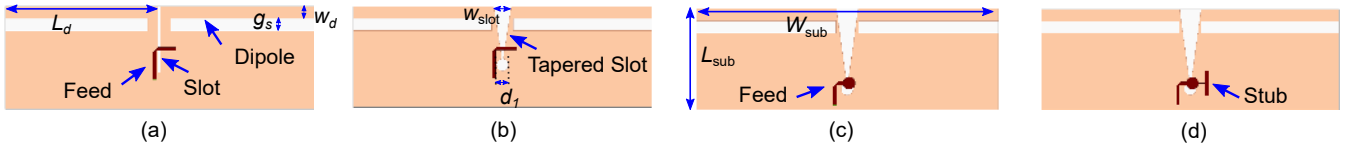

FIGURE 1. Design evolution of a dipole: (a) excited via rectangular slot, (b) excited via tapered slot, (c) tapered slot with modified feeding, and (d) modified feeding with stub.

aperture antenna which increased the overall size. In short, new promising antenna structures should still be explored to match the requirements of the integrated wireless communication system.

In this work, an integrated antenna system is proposed for sub-6 GHz and mm-wave applications. The key element of the design is a dipole antenna, which has dual-feature. Firstly, it works as a conventional dipole operating at 3.6 GHz and fed from a tapered slot. This tapered slot also operates as an end-fire high gain antenna at mm-wave band. Thus, it also has a dual-feature, i.e., used as a feeding component for the dipole at sub-6 GHz and as an antenna at mm-wave band. This feature of the structure provides an extremely large operating frequency ratio, which makes the design unique. The utilization of a single shared feed is also presented in [21] for a slot and printed inverted-F antenna to achieve a compact multi-bands antenna. However, it only covers 4G bands with very small frequency ratio of about 2.1. Secondly in the proposed design, the dipole is also used as an antenna footprint for two mm-wave tapered slot arrays. The proposed design can operate at several bands (1.9 GHz, 3.6 GHz, 5.2 GHz, and 28 GHz) and provides three high gain directive beams at 28 GHz, which covers 120^o of the free space in θ-direction. In summary, by incorporating the multi-functionality of different structures, the proposed antenna can achieve multi-band operation and large space coverage using a compact footprint.

II. DESIGN EVOLUTION

For the ultimate aim of achieving a common-aperture (or shared-aperture) antenna structure with larger space coverage at mm-wave band, a new design approach is proposed. The entire antenna design is a combination of a dipole, tapered slot, and rectangular slot antennas. This section will explain the design evolution, starting from the sub-6 GHz antenna configuration, followed by the incorporation of mm-wave antenna. Based on this, a design guideline is provided at the end.

In order to validate the proposed design approach, Rogers RO-5880 substrate, which is an efficient material at both microwave and mm-wave bands, is chosen. The length of the substrate is kept $L_{\text{sub}} = 25$ mm, while the width is set to $W_{\text{sub}} = 75$ mm, which matches the dimensions of modern mobile terminals to prove the proposed concept. However, the proposed concept and dimensions of the designs can be tailored to any specific application/configuration, such as mobile terminals, tablets, access points, and WLAN. The substrate has dielectric constant $(\epsilon_r) = 2.2$, loss tangent $(\tan\delta) = 0.0009$ at 10 GHz, and thickness $(t) = 0.254$ mm.

A. SUB-6 GHZ ANTENNA CONFIGURATION

First, a modified printed dipole fed by a rectangular slot is considered (Figure 1(a)). The dipole dimension is selected to operate at 3.6 GHz band. The total length of the dipole is 75 mm (about one λ long, λ is a free space wavelength at 3.6 GHz) considering a mobile device width dimension. To excite the dipole, an integrated balun, which consists of a tapered 50 Ω L-shaped feeding structure and a rectangular slot, is implemented. This is a classical method to excite a printed dipole as shown in [22], [23]. The length of the slot is chosen as a quarter-wavelength.

Since the dipole will be modified to achieve common-aperture configuration, a parametric study is first conducted to understand and confirm the behaviour of critical parameters. It is noted that the two arms of the dipole will be utilized to integrate two mm-wave antennas, which will be shown in the next section. It is verified that the width (w_d) and the spacing (g_s) do not have a significant effect on the performance (not shown here for brevity), while the L_d can tune the resonance (see Figure 2).

The rectangular slot is then modified to a tapered slot as shown in Figure 1(b). Here, the antenna can be still viewed as a dipole, excited by a tapered slot [24], which provides an extra degree of freedom in improving the impedance matching and enhancing the bandwidth at 3.6 GHz. Interestingly, this tapered slot can also operate as a Vivaldi antenna at mm-wave frequency band with high gain. By doing so, an extremely large frequency ratio is achieved. Although the wideband operations were achieved by using a dipole and slot antennas in [24], it was not an integrated antenna design and covered only microwave band, while the proposed design has the capabilities to cover several bands at microwave and mm-wave bands. The initial parameters (L_{slot}, w_{slot}, and d_{slot}) are formulated based on the procedure demonstrated in [20]. The performance of the dipole when excited with the original rectangular slot and the tapered slot is compared in Figure 3(a). The tapered slot provides larger -6-dB impedance matching bandwidth of about 150 MHz. Furthermore, the simulations have also been carried out to analyze critical parameters (width (w_{slot}) and diameter (d_{slot}) of the circular stub) of the tapered slot. Figs. 3(b) and (c) shows the reflection coefficients for different values of w_{slot} and d_{slot}. It can be observed that decreasing w_{slot} or increasing d_{slot} lowers the resonance frequency as the overall antenna

This article has been accepted for publication in a future issue of this journal, but has not been fully edited. Content may change prior to final publication. Citation information: DOI 10.1109/ACCESS.2020.3034887, IEEE Access

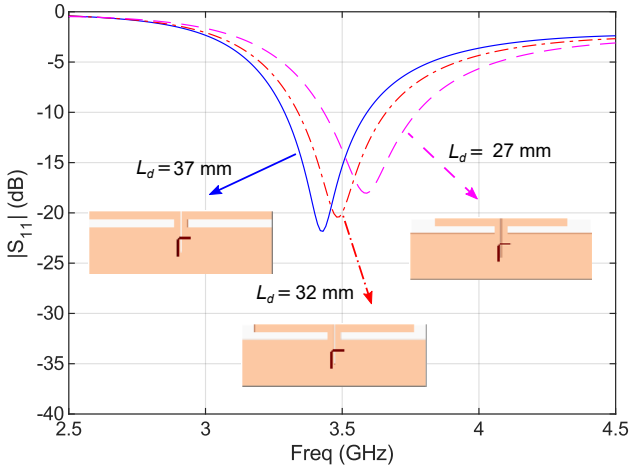

FIGURE 2. The simulated $|S_{11}|$ for different values of L_d.

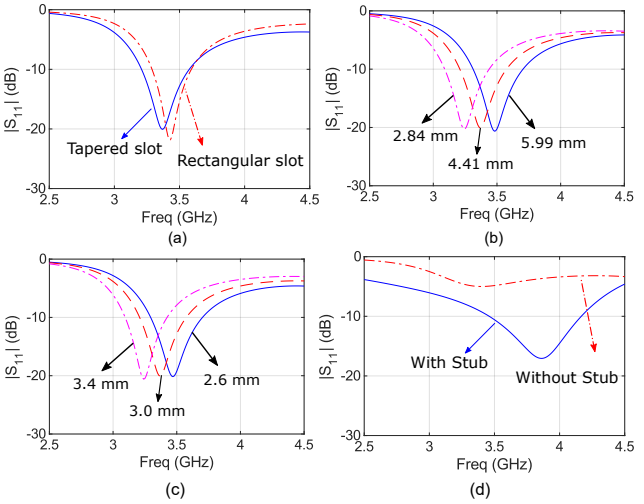

FIGURE 3. The simulated $|S_{11}|$ for (a) rectangular and tapered slot, for different values of (b) w_{slot} (c) d_{slot}, and for (d) modified feed with and without stub.

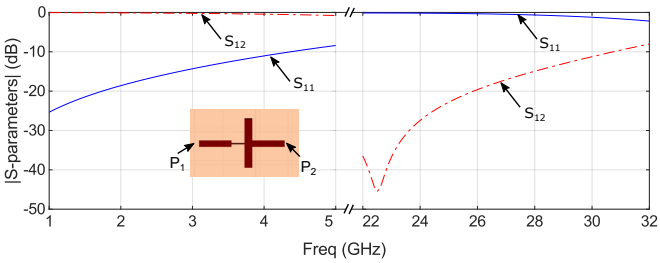

FIGURE 4. The simulated performance of a stub (working as a LPF) at sub-6 GHz and mm-wave bands.

size increases.

Next, the feeding structure of the dipole is modified and relocated to the edge of the tapered slot as shown in Figure 1(c). The objective here is to use the tapered slot as an end-fire high-gain antenna at mm-wave band (details are given in Section II.B). Therefore, the feeding structure should be placed at the edge of the tapered slot and terminated with a circular stub for wideband matching [20]. However, this feeding structure significantly affects the impedance matching at 3.6 GHz as shown in Figure 3(d) (red dot-dashed curve). This problem is solved by incorporating a stub along with the feeding as shown in Figure 1(d). This stub is actually designed as a low pass filter (LPF) using the stepped-impedance technique [25], [26]. As a LPF, at low frequency, the stub acts as impedance matching circuit while it does not affect the performance at mm-wave band. Figure 3(d) shows the improved impedance matching at 3.6 GHz band after adding the LPF (blue solid curve). It can be seen that the dipole resonates at 3.8 GHz with a -6-dB impedance bandwidth of about 1 GHz from 3.4 to 4.4 GHz. The performance of the stub as a filter at sub-6 GHz and mm-wave bands is also shown in Figure 4.

B. COMPLETE COMMON-APERTURE SUB-6 GHZ AND MM-WAVE ANTENNA SYSTEM

The main goal is to design a multi-beam antenna structure operating at 28 GHz by using the footprint of sub-6 GHz dipole antenna. Hence, the overall antenna footprint remains the same. This feature of the proposed work makes it a promising candidate for modern compact multi-band wireless devices, i.e. handheld devices.

The mm-wave antenna starts by considering the design discussed in Section II.A (Figure 1(d)). Since, the width (w_d) does not alter the performance of the dipole significantly, it is increased from 3 mm to 9 mm (see Figure 5(a)) to accommodate two mm-wave arrays. With this structure, multiple beams pointing at different locations in the end-fire direction via multi-port antenna structure will be designed. First, the parameters of the main tapered slot and its feeding structure are fine-tuned to improve the performance at both frequency bands. Here, d_1 and d_2 are the most critical parameters for the impedance matching bandwidth at mm-wave band. However, these parameters do not significantly affect the performance of the dipole. Therefore, by appropriately choosing the value of these parameters, satisfactory performance of the dipole antenna at 3.6 GHz band and the tapered slot at mm-wave band can be achieved. The simulated performance of the optimized design ($d_1 = 3.2$ mm and $d_2 = 2.5$ mm) is shown in Figure 5. The design works as a dipole antenna at 3.6 GHz with peak realized gain of 4 dBi and as a tapered slot antenna at 28 GHz with a peak realized gain of 8 dBi.

Next, two mm-wave tapered slot arrays (Ant. 2 and Ant. 3) are placed over the dipole arms (see Figure 6). The fundamental element of each mm-wave array is also the tapered slot. Each array is tilted by $\pm 25^o$ along y-axis to provide large space coverage as a multi-beam antenna system. The design procedure is the same as the main tapered slot. While the lengths are kept smaller due to limited space of dipole arms, with the two elements in each array, the gain of each tilted array is comparable to the main broadside slot. The 2D

This article has been accepted for publication in a future issue of this journal, but has not been fully edited. Content may change prior to final publication. Citation information: DOI 10.1109/ACCESS.2020.3034887, IEEE Access

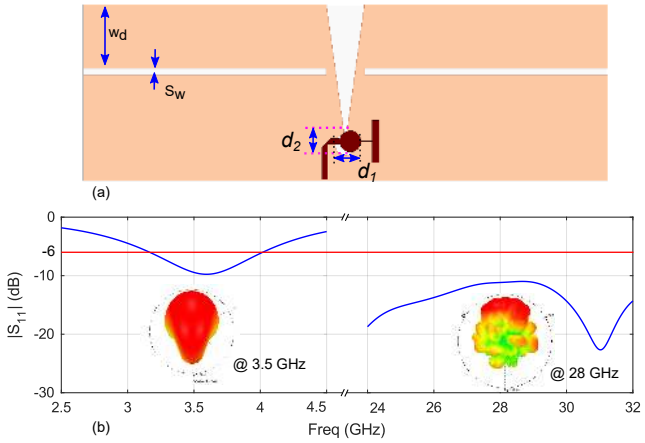

FIGURE 5. The design showing performance of the dipole and tapered slot antennas at sub-6 GHz and mm-wave bands. (a) The geometry and (b) the simulated reflection coefficients and 3D radiation patterns in terms of realized gain.

normalized radiation patterns in terms of peak realized gain of the main tapered slot antenna (Ant. 1) and two mm-wave arrays (Ant. 2 and Ant. 3) are shown in Figure 7. It can be seen that it covers an angle of 120^o in θ-direction with the maximum and minimum peak realized gains of 8 dBi and 6 dBi, respectively.

The feeding structure of the mm-wave tapered slot arrays is designed based on a tapered T-junction power divider (PD) as shown in Fig 6. The PD consists of two 100-Ω (output ports of PD), which directly excites the tapered slots, and a 50-Ω, which is used on the input side of the PD, transmission lines. Both power dividers are rotated by $\pm 25^o$ in order to excite the tilted tapered slot arrays (Ant. 2 and Ant. 3). Due to the presence of Ant. 2 and Ant. 3, the performances of the dipole at 3.6 GHz and the tapered slot at 28 GHz slightly change due to the change in dipole arm's shape and the coupling effect of these slots. Thus, the whole design is slightly fine-tuned to achieve satisfactory performance (shown in Section III). The final optimized parameters are given in the caption of Figure 6.

At this stage, we achieve a compact common-aperture antenna system operates at 5G mm-wave and sub-6 GHz bands. In fact, the proposed geometry is open for additional bands at sub-6 GHz although it is not the main target of the paper. As an example for demonstration purpose, the 1.9 GHz and 5.2 GHz bands can be achieved using a conventional rectangular slot antenna (Ant. 4), which is formed between the dipole arm and ground plane as shown in Figure 6. It is fed via 50 Ω transmission line. The slot antenna is optimized to operate at 1.9 GHz 4G-LTE band and 5.2 GHz WLAN band. As discussed in [27], the two lowest-order modes of an open slot ($TE_{0.5,0}$ and $TE_{1.5,0}$) are excited here. The slot resonates at 1.9 GHz and 5.2 GHz when the length s_L is about $\lambda_g/4$ and $3\lambda_g/4$, respectively (λ_g is an effective wavelength at 1.9 GHz). The performance of the slot antenna in terms of S-parameters will be reported in Section III.A.

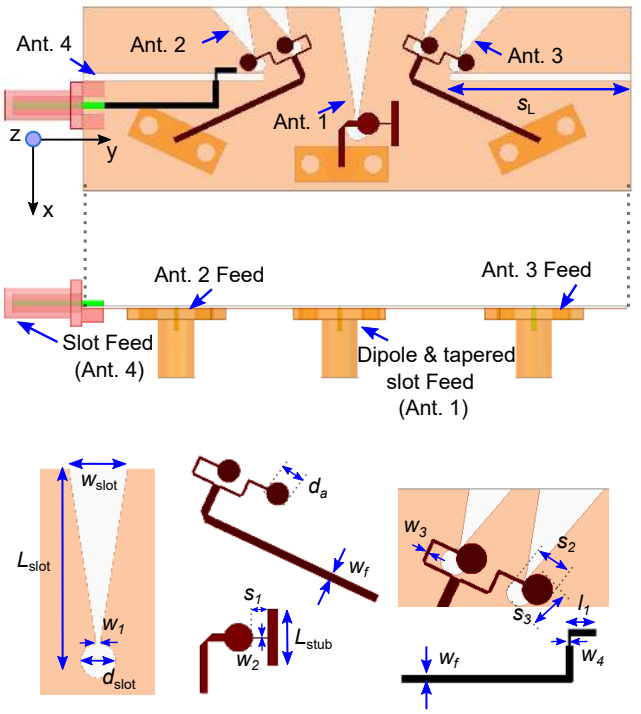

FIGURE 6. The entire geometry of a sub-6 GHz and mm-wave band common-aperture 5G antenna system. The optimized parameters in millimeters (mm) are as follows: L_{sub}= 25, W_{sub}= 75, t_{sub}= 0.254, d_{slot}= 1.3, W_{slot}= 5.1, L_{slot}= 18.16, W_f= 0.783, L_{stub}= 6, s_1= 1.65, d_1= 4.5, d_2= 3.76, w_d= 9, L_d= 37.5, w_1=0.5, w_2= 0.1, w_3= 0.227, w_4=0.3, s_2= 3.37, s_3= 3.2, s_w= 1, s_L= 24.75, d_a= 2.3, and l_1= 3.

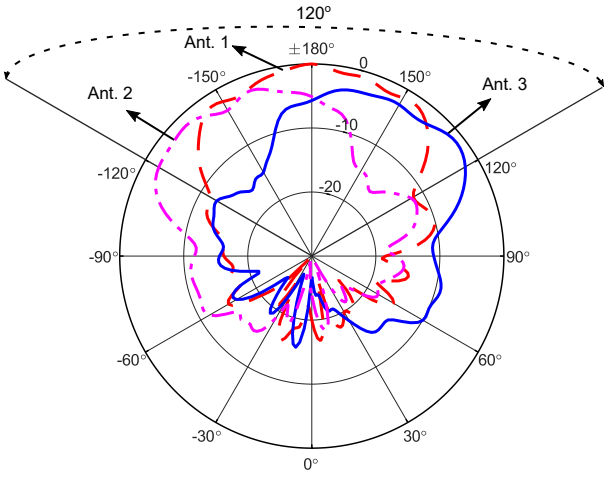

FIGURE 7. The 2D simulated radiation patterns at $\theta = 90^o$ for Ant. 1-Ant. 3 at 28 GHz.

C. DESIGN PROCEDURE

Since the antenna system is a combination of different geometries, which form a common-aperture sub-6 GHz and mm-wave antenna, a step-by-step design procedure is demonstrated below.

- Select the targeted sub-6 GHz frequency, i.e., 3.6 GHz.
- Choose the length of a dipole, i.e. L_d by $\lambda/2$.

This article has been accepted for publication in a future issue of this journal, but has not been fully edited. Content may change prior to final publication. Citation information: DOI 10.1109/ACCESS.2020.3034887, IEEE Access

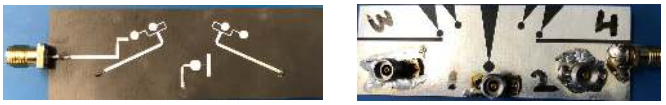

(a) (b)

FIGURE 8. Photograph of a fabrication prototype. (a) Top and (b) bottom views.

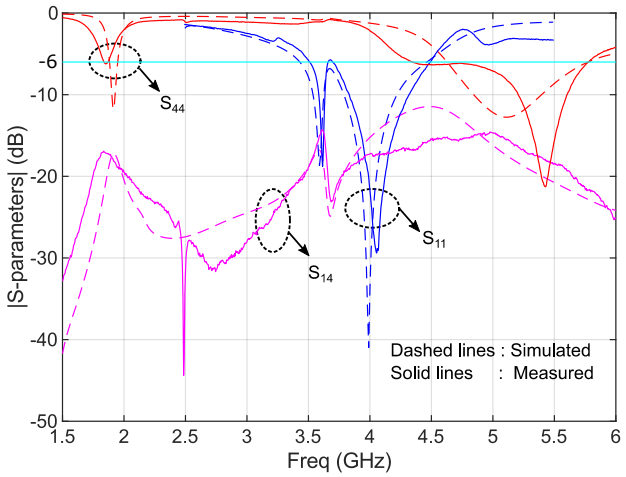

FIGURE 9. The simulated and measured S-parameters for Ant. 1 and Ant. 4 at sub-6 GHz band.

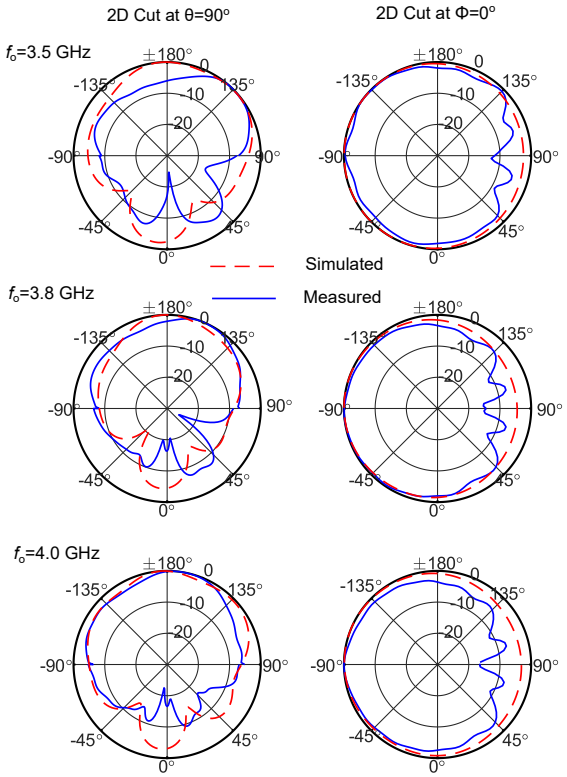

FIGURE 10. The simulated and measured normalized 2D radiation patterns at 3.5 GHz, 3.8 GHz, and 4.0 GHz for the dipole (Ant. 1).

- Excite the dipole with a quarter wavelength long rectangular slot.
- Replace the rectangular slot with a tapered slot. The geometry of the tapered slot must be designed based on a procedure discussed in [20], [28] because it will also be used as a tapered slot antenna at 28 GHz.
- Design and optimize a feeding structure along with low pass filter (stub) that can excite the whole structure as a dipole antenna at 3.6 GHz and a tapered slot antenna at 28 GHz.
- Add two mm-wave tapered slot arrays over the dipole arms.
- Fine-tune the design to have satisfactory performance at both 3.6 GHz and 28 GHz band.
- As the dipole arm and ground plane produce an additional rectangular slot, a feeding structure can be designed to excite that slot at the two resonances 1.9 GHz and 5.2 GHz.

III. EXPERIMENTAL RESULTS AND DISCUSSIONS

All simulations and modeling of the antenna design are carried out using the ANSYS High Frequency Structure Simulator (HFSS). The complete optimized geometry of the proposed design is shown in Figure 6, while the fabrication photograph is shown in Figure 8. The performance of the design is discussed below.

A. PERFORMANCE AT SUB-6 GHZ BAND

The simulated and measured S-parameters of sub-6 GHz bands are presented in Figure 9. It can be seen from the results that the Ant. 1 and Ant. 4 have good reflection coefficients of better than -6 dB at 3.6 GHz from 3.4-4.4 GHz and at 1.9 GHz from 1.87-1.94 GHz and at 5.2 GHz from 4.6-5.6 GHz, respectively. While the main target of the proposed work is to present a shared aperture antenna that covers 3.6 GHz band with wide impedance matching bandwidth and 28 GHz band with multiple beams, the rectangular slot antenna is only an additional feature of the proposed geometry, which provides a narrow band at 1.9 GHz and a wide band at 5.2 GHz. Nevertheless, the band at 1.9 GHz can also be widened by incorporating active components [19], [29]. The isolation between Ant. 1 and Ant. 4 is more than 15 dB across the whole targeted bands.

Figure 10 shows 2D normalized simulated and measured radiation patterns at $\theta = 90^o$ and $\phi = 0^o$ for Ant. 1 at different frequencies, i.e. at 3.5 GHz, 3.8 GHz, and 4.0 GHz. The results show that Ant. 1 has wide beamwidth, which is desirable at low frequency applications. Moreover, the consistent radiation patterns over a wide range of frequencies verify the wideband characteristics of Ant. 1 at sub-6 GHz band.

This article has been accepted for publication in a future issue of this journal, but has not been fully edited. Content may change prior to final publication. Citation information: DOI 10.1109/ACCESS.2020.3034887, IEEE Access

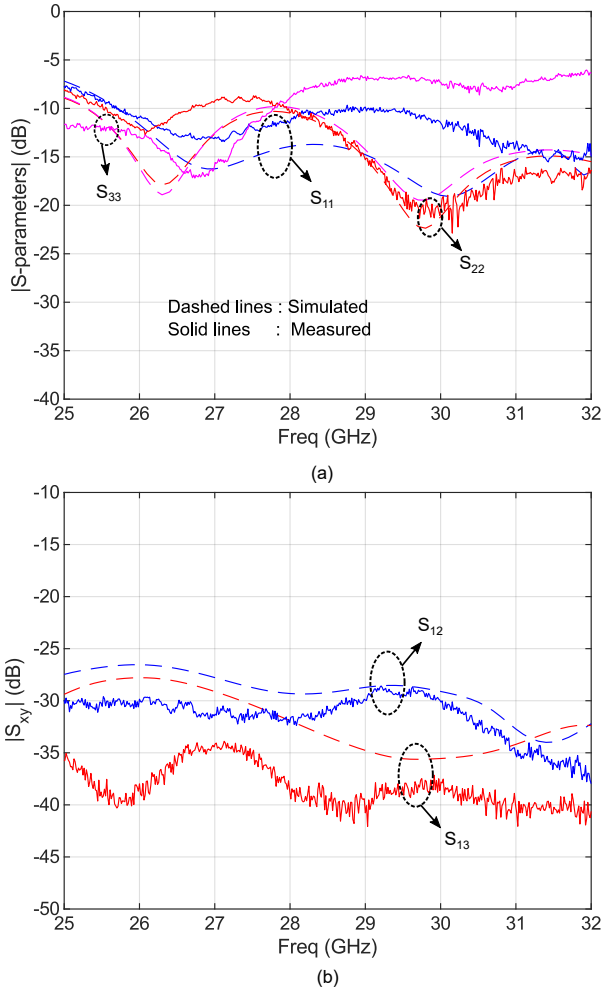

FIGURE 11. The simulated and measured S-parameters for Ant. 1, Ant. 2, and Ant. 3 at mm-wave bands. (a) Reflection coefficients and (b) isolation.

B. PERFORMANCE AT MM-WAVE BAND

The simulated and measured reflection coefficients at mm-wave band for Ant. 1, Ant. 2, and Ant. 3 are presented in Figure 11(a). The results show that Ant. 1-Ant. 3 cover 28 GHz mm-wave band with a very wide bandwidth from 25 GHz to 32 GHz. A slight discrepancy between simulated and measured results especially for Ant. 3 is observed. It is attributed to the soldering the connectors at an in-house facility. Nevertheless, the results still show -7 dB impedance matching across the whole band.

The simulated and measured isolation between Ant. 1-Ant. 2 and Ant. 1-Ant. 3 are shown in Figure 11(b). The maximum isolation of 26 dB, which is acceptable for mobile applications [7], is observed between Ant. 1 and Ant 2.

For the radiation patterns measurements at mm-wave band, one antenna (Ant. 1-Ant. 3) is excited at a time, while others are terminated with 50 Ω matched load. For real applications, i.e. mobile phone, a front-end module (FEM) reported in [7] can be used. The simulated and measured 2D radiation patterns for Ant. 1-Ant. 3 are compared in Figure 12 and

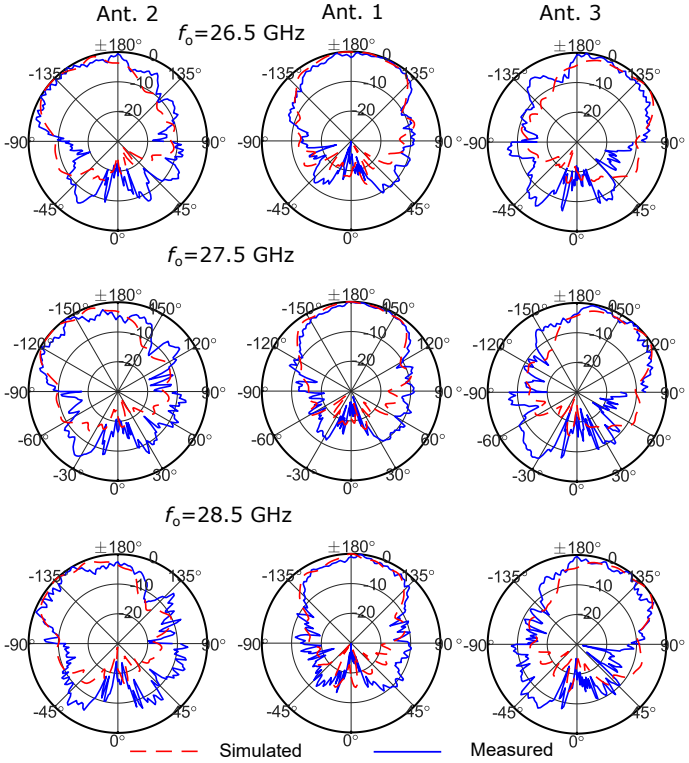

FIGURE 12. The simulated and measured normalized 2D radiation patterns at $\theta = 90^o$ for Ant. 1, Ant. 2, and Ant. 3 at 26.5 GHz, 27.5 GHz, and 28.5 GHz.

Figure 13 at $\theta = 90^o$ and $\phi = 0^o$, respectively. The results are presented at different frequencies, i.e. 26.5 GHz, 27.5 GHz, and 28.5 GHz showing a good agreement between simulated and measured results. As expected, beam-width is narrower for Ant. 1 at mm wave band compared to sub-6 GHz band. Whereas, Ant. 2 and Ant. 3 consist of an array of two tapered slots that provide wider beam-width in $\phi-$direction and narrow beam-width in $\theta-$direction. Moreover, all the patterns follow the same trend at all presented frequencies. In particular, the patterns at $\theta = 90^o$ verify that Ant. 1-Ant. 3 provide 120^o beam coverage for a wide range of frequencies.

The simulated and measured realized gain and efficiency at both sub-6 GHz and mm-wave bands are presented in Figure 14(a) and Figure 14(b), respectively. The Ant. 1 provides a maximum gain of 4 dBi and 8 dBi at both of respective bands. While Ant. 2 and Ant. 3 have a maximum gain of 7 dBi. The 7-10 dBi gain, which is acceptable for terminal antennas, is common in the literature [7], [17], [30]. Overall, measured efficiency in the range of 65%-90% is achieved at both bands. A 1.5 dBi difference between the simulated and measured gains is observed at sub-6 GHz band. This difference is attributed to the error in measurement and the effects of cables and connectors, which slightly increase the directivity. For higher frequency range, the measured efficiency is slightly less than the simulated one due to the higher loss at mm-wave frequencies.

To see the effect of a large ground plane over the perfor-

This article has been accepted for publication in a future issue of this journal, but has not been fully edited. Content may change prior to final publication. Citation information: DOI 10.1109/ACCESS.2020.3034887, IEEE Access

TABLE 1. Comparison between the proposed and recently reported designs.

Figure of merits	**Proposed work**	[7]	[11]	[17]	[18]	[30]
Covered microwave bands (GHz)	1.9, 3.5, 5.2	None	2.0, 3.5, 5.2	3.5	2.4, 5.2	0.8, 2.0
Covered mm-wave bands (GHz)	28	28, 38	28, 38	28	60	28
Realized gain (dBi) at mm-wave band	8	8	11	10	12	9
Beam switching mechanism at mm-wave band	multi-port multi-antenna	multi-port multi-antenna	array design	array design	single port leaky wave antenna	array design
Beam coverage at mm-wave band	± 60	± 90	N/A	± 34	± 36	± 50

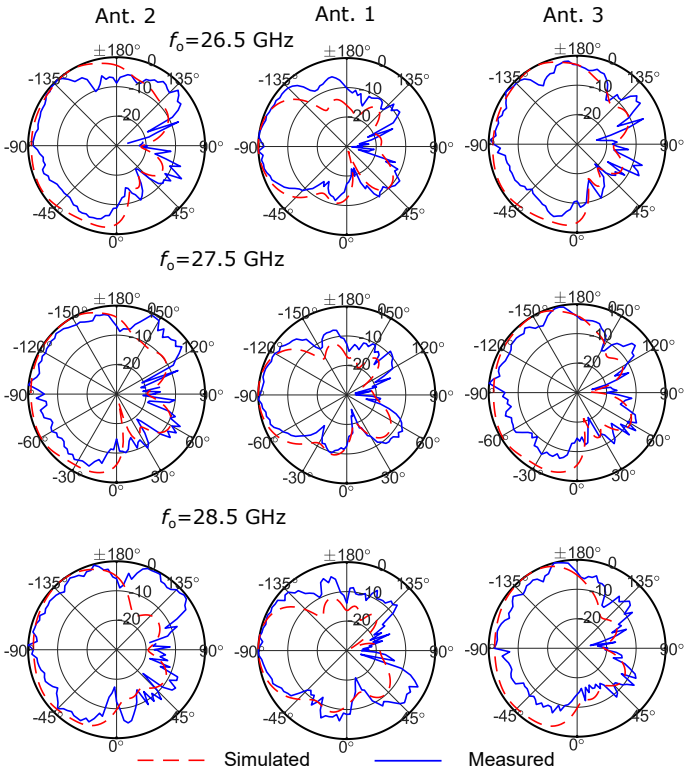

FIGURE 13. The simulated and measured normalized 2D radiation patterns at $\phi = 0^o$ for Ant. 1, Ant. 2, and Ant. 3 at 26.5 GHz, 27.5 GHz, and 28.5 GHz.

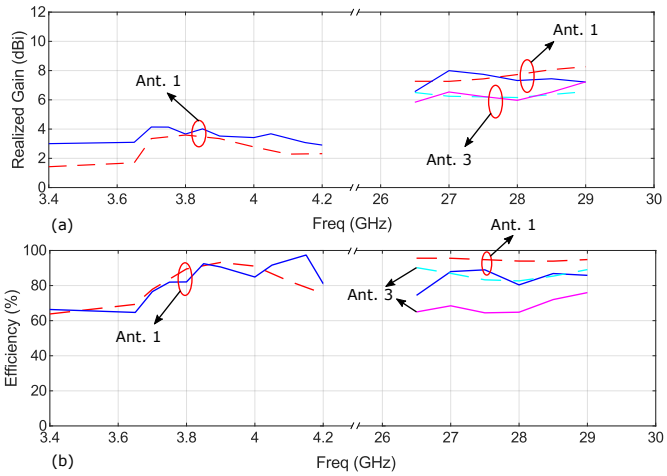

FIGURE 14. The simulated and measured peak realized gain and efficiency at sub-6 GHz and mm-wave bands. Simulated:dashed-lines; measured:solid-lines.

mance of the proposed design for practical applications, i.e. mobile terminals, one possible scenario is demonstrated in Figure 15, where the length of the ground plane is extended to 150 mm. The design is simulated and its S-parameters are experimentally validated. The simulated and measured S-parameters are shown in Figure 16. It is clear from the results that the performance of the proposed design is not significantly dependent on the ground plane as most of antenna elements have directive pattern and the design still covers the same sub-6 GHz (1.9 GHz, 3.6 GHz, and 5.2 GHz) and mm-wave (28 GHz) bands. The results also show a good agreement between simulation and measurements.

IV. COMPARISON WITH THE RELATED WORK

Table 1 shows a comparison between the proposed and related recent works based on covered microwave and mm-wave bands and realized gain, beam switching mechanism, and beam coverage at mm-wave band. It can be noticed that the proposed design covers several frequency bands at microwave and mm-wave. The proposed design also has a wider beam coverage, which is about $\pm 60^o$ at mm-wave, than [17], [18], [30]. Although [7] provides more wider beam coverage and [11] covers similar frequency bands, [7] is not a common aperture and does not support microwave frequency bands, whereas [11] does not have beam scanning. Overall, the proposed design has a comparable realized gain of 8 dBi with [7], [17], [30].

V. CONCLUSION

A common-aperture 5G antenna system has been proposed in this work. The main goal is to present a compact antenna array architecture that operates at multi-bands, i.e. sub-6 GHz at 3.6 GHz and mm-wave at 28 GHz. A dual-functional tapered slot is designed and used to excite a dipole antenna at 3.6 GHz. That tapered slot also works as an end-fire high-gain antenna at 28 GHz. Due to a single feeder for both antennas, an extremely large frequency ratio is achieved. In addition, two tilted tapered slot mm-wave arrays are designed over the dipole arms, making the dipole also dual-functional. The radiation pattern beams from the tapered slot antenna and the mm-wave arrays can scan an area of 120^o with a realized gain of 8 dBi. Such configuration makes the design compact

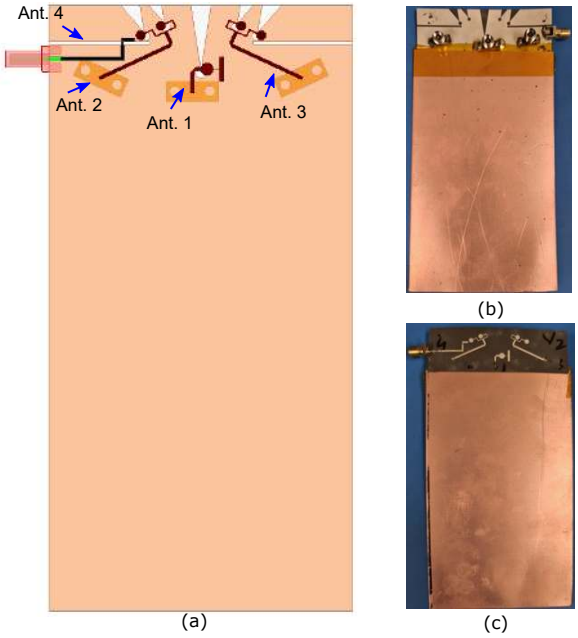

FIGURE 15. The geometry of the design with a large ground plane. (a) Simulated model top view and fabrication prototype (b) top and (c) bottom views.

and hence, a good candidate for modern multi-bands wireless terminals.

REFERENCES

[1] T. S. Rappaport, S. Sun, R. Mayzus, H. Zhao, Y. Azar, K. Wang, G. N. Wong, J. K. Schulz, M. Samimi, and F. Gutierrez, "Millimeter Wave Mobile Communications for 5G Cellular: It Will Work!," IEEE Access, vol. 1, pp. 335–349, 2013.

[2] J. G. Andrews, S. Buzzi, W. Choi, S. V. Hanly, A. Lozano, A. C. K. Soong, and J. C. Zhang, "What will 5g be?," IEEE Journal on Selected Areas in Communications, vol. 32, no. 6, pp. 1065–1082, 2014.

[3] Federal Communications Commission (FCC), "The FCC's 5G FAST Plan, Spectrum." https://www.fcc.gov/5G.

[4] N. Ojaroudiparchin, M. Shen, S. Zhang, and G. F. Pedersen, "A Switchable 3-D-Coverage-Phased Array Antenna Package for 5G Mobile Terminals," IEEE Antennas and Wireless Propagation Letters, vol. 15, pp. 1747–1750, 2016.

[5] S. Zhang, X. Chen, I. Syrytsin, and G. F. Pedersen, "A Planar Switchable 3-D-Coverage Phased Array Antenna and Its User Effects for 28-GHz Mobile Terminal Applications," IEEE Transactions on Antennas and Propagation, vol. 65, no. 12, pp. 6413–6421, 2017.

[6] M. Khalily, R. Tafazolli, P. Xiao, and A. A. Kishk, "Broadband mm-Wave Microstrip Array Antenna With Improved Radiation Characteristics for Different 5G Applications," IEEE Transactions on Antennas and Propagation, vol. 66, no. 9, pp. 4641–4647, 2018.

[7] C. Di Paola, S. Zhang, K. Zhao, Z. Ying, T. Bolin, and G. F. Pedersen, "Wideband Beam-Switchable 28 GHz Quasi-Yagi Array for Mobile Devices," IEEE Transactions on Antennas and Propagation, vol. 67, no. 11, pp. 6870–6882, 2019.

[8] C. Di Paola, S. Zhang, and G. F. Pedersen, "Hybrid high gain antenna systems, devices, and methods," July 11 2019. US Patent App. 16/240,399.

[9] Y. Hsu, T. Huang, H. Lin, and Y. Lin, "Dual-Polarized Quasi YagiâĂŞUda Antennas With Endfire Radiation for Millimeter-Wave MIMO Terminals," IEEE Transactions on Antennas and Propagation, vol. 65, no. 12, pp. 6282–6289, 2017.

[10] W. Hong, "Solving the 5G Mobile Antenna Puzzle: Assessing Future Directions for the 5G Mobile Antenna Paradigm Shift," IEEE Microwave Magazine, vol. 18, pp. 86–102, Nov 2017.

[11] Y. Liu, Y. Li, L. Ge, J. Wang, and B. Ai, "A Compact Hepta-Band Mode-Composite Antenna for Sub (6, 28, and 38) GHz Applications," IEEE Transactions on Antennas and Propagation, vol. 68, no. 4, pp. 2593–2602, 2020.

[12] T. Li and Z. N. Chen, "Shared-surface dual-band antenna for 5g applications," IEEE Transactions on Antennas and Propagation, vol. 68, no. 2, pp. 1128–1133, 2020.

[13] Y. Sun and K. W. Leung, "Substrate-Integrated Two-Port Dual-Frequency Antenna," IEEE Transactions on Antennas and Propagation, vol. 64, pp. 3692–3697, Aug 2016.

[14] D. Wang and C. H. Chan, "Multiband Antenna for WiFi and WiGig Communications," IEEE Antennas and Wireless Propagation Letters, vol. 15, pp. 309–312, 2016.

[15] T. Zhihong, Y. P. Zhang, C. Luxey, A. Bisognin, D. Titz, and F. Ferrero, "A Ceramic Antenna for Tri-Band Radio Devices," IEEE Transactions on Antennas and Propagation, vol. 61, pp. 5776–5780, Nov 2013.

[16] L. Zhang, K. Y. See, B. Zhang, and Y. P. Zhang, "Integration of Dual-Band Monopole and Microstrip Grid Array for Single-Chip Tri-Band Application," IEEE Transactions on Antennas and Propagation, vol. 61, pp. 439–443, Jan 2013.

[17] J. Lan, Z. Yu, J. Zhou, and W. Hong, "An Aperture-Sharing Array for 3.5/28 GHz Terminals with Steerable Beam in Millimeter Wave Band," IEEE Transactions on Antennas and Propagation, pp. 1–1, 2019.

[18] Y. R. Ding and Y. J. Cheng, "A Tri-Band Shared-Aperture Antenna for (2.4, 5.2) GHz Wi-Fi Application With MIMO Function and 60 GHz Wi-Gig Application With Beam-Scanning Function," IEEE Transactions on Antennas and Propagation, vol. 68, no. 3, pp. 1973–1981, 2020.

[19] M. Ikram, E. A. Abbas, N. Nguyen-Trong, K. H. Sayidmarie, and A. Abbosh, "Integrated Frequency-Reconfigurable Slot Antenna and Connected Slot Antenna Array for 4G and 5G Mobile Handsets," IEEE Transactions on Antennas and Propagation, vol. 67, no. 12, pp. 7225–7233, 2019.

[20] M. Ikram, N. Nguyen-Trong, and A. Abbosh, "Multiband MIMO Mi-

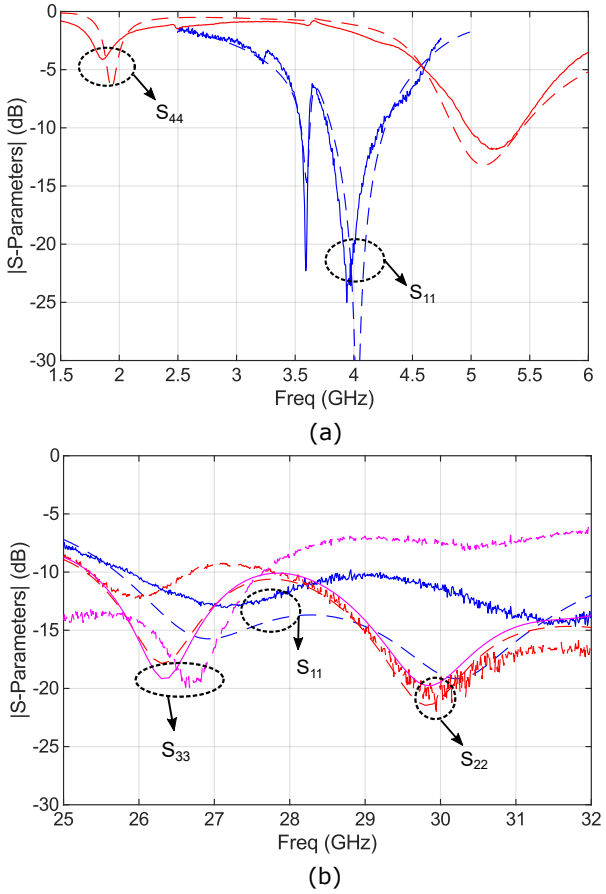

FIGURE 16. The simulated and measured S-parameters for Ant. 1 to Ant. 4 at (a) sub-6 GHz and (b) mm-wave bands after enlarging the ground plane. Simulated:dashed-lines; measured:solid-lines.

crowave and Millimeter Antenna System Employing Dual-Function Tapered Slot Structure," IEEE Transactions on Antennas and Propagation, vol. 67, no. 8, pp. 5705–5710, 2019.

[21] J. Anguera, I. Sanz, J. Mumbru, and C. Puente, "Multiband handset antenna with a parallel excitation of pifa and slot radiators," IEEE Transactions on Antennas and Propagation, vol. 58, no. 2, pp. 348–356, 2010.

[22] Huey-Ru Chuang and Liang-Chen Kuo, "3-D FDTD design analysis of a 2.4-GHz polarization-diversity printed dipole antenna with integrated balun and polarization-switching circuit for WLAN and wireless communication applications," IEEE Transactions on Microwave Theory and Techniques, vol. 51, no. 2, pp. 374–381, 2003.

[23] R. Li, T. Wu, B. Pan, K. Lim, J. Laskar, and M. M. Tentzeris, "Equivalent-Circuit Analysis of a Broadband Printed Dipole With Adjusted Integrated Balun and an Array for Base Station Applications," IEEE Transactions on Antennas and Propagation, vol. 57, no. 7, pp. 2180–2184, 2009.

[24] Tzyh-Ghuang Ma and Shyh-Kang Jeng, "A printed dipole antenna with tapered slot feed for ultrawide-band applications," IEEE Transactions on Antennas and Propagation, vol. 53, no. 11, pp. 3833–3836, 2005.

[25] J. Ni and J. Hong, "Compact Continuously Tunable Microstrip Low-Pass Filter," IEEE Transactions on Microwave Theory and Techniques, vol. 61, no. 5, pp. 1793–1800, 2013.

[26] E. Al Abbas, M. Ikram, A. T. Mobashsher, and A. Abbosh, "MIMO Antenna System for Multi-Band Millimeter-Wave 5G and Wideband 4G Mobile Communications," IEEE Access, vol. 7, pp. 181916–181923, 2019.

[27] M. Ikram, N. Nguyen-Trong, and A. Abbosh, "Hybrid Antenna using Open-Ended Slot for Integrated 4G/5G Mobile Application," IEEE Antennas and Wireless Propagation Letters, pp. 1–1, 2020.

[28] K. Ebnabbasi, D. Busuioc, R. Birken, and M. Wang, "Taper Design of Vivaldi and Co-Planar Tapered Slot Antenna (TSA) by Chebyshev Transformer," IEEE Transactions on Antennas and Propagation, vol. 60, no. 5, pp. 2252–2259, 2012.

[29] M. Stanley, Y. Huang, H. Wang, H. Zhou, Z. Tian, and Q. Xu, "A Novel Reconfigurable Metal Rim Integrated Open Slot Antenna for Octa-Band Smartphone Applications," IEEE Transactions on Antennas and Propagation, vol. 65, pp. 3352–3363, July 2017.

[30] M. M. Samadi Taheri, A. Abdipour, S. Zhang, and G. F. Pedersen, "Integrated Millimeter-Wave Wideband End-Fire 5G Beam Steerable Array and Low-Frequency 4G LTE Antenna in Mobile Terminals," IEEE Transactions on Vehicular Technology, vol. 68, pp. 4042–4046, April 2019.